

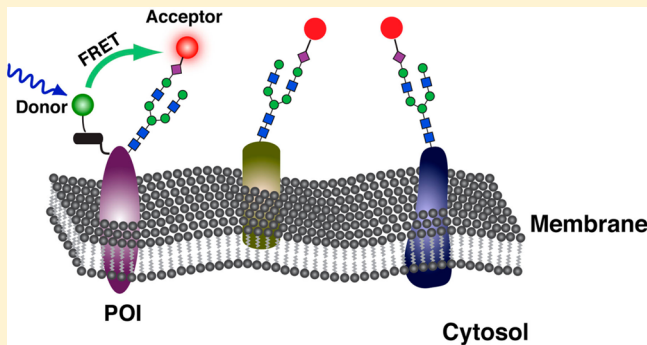
## A Cis-Membrane FRET-Based Method for Protein-Specific Imaging of Cell-Surface Glycans

Wei Lin, Yifei Du, Yuntao Zhu, and Xing Chen\*

Beijing National Laboratory for Molecular Sciences, Department of Chemical Biology, College of Chemistry and Molecular Engineering, Synthetic and Functional Biomolecules Center, and Peking-Tsinghua Center for Life Sciences, Peking University, Beijing 100871, P.R. China

 Supporting Information

**ABSTRACT:** Metabolic labeling of glycans with chemical reprotores (e.g., alkyne or azide) in conjunction with bioorthogonal chemistry is a powerful tool for imaging glycome; however, this method lacks protein-specificity and therefore is not applicable to imaging glycosylation of a specific protein of interest (POI). Here we report the development of a cis-membrane FRET-based methodology that allows protein-specific imaging of glycans on live cells. We exploit metabolic glycan labeling in conjunction with site-specific protein labeling to simultaneously install a FRET acceptor and a donor onto the glycans and the extracellular terminal of the protein of interest, respectively. The intramolecular donor–acceptor distance for the POI falls within the range for effective FRET, whereas the intermolecular FRET is disfavored since the excess acceptors on other proteins are distant from the donor. We demonstrated the capability of this cis-membrane FRET imaging method by visualizing the sialylation of several important cell surface receptors including integrin  $\alpha_5\beta_1$ , epidermal growth factor receptor, and transforming growth factor-beta receptor type I. Furthermore, our imaging experiments revealed that the sialylation might be important for  $\beta_1$  integrin activation. Our methodology should enable the live-cell studies on how glycosylation regulates the functions and dynamics of various cell-surface proteins.



### INTRODUCTION

In vertebrates, most of the cell-surface receptors are post-translationally modified with glycans. Protein glycosylation plays essential roles in regulating the dynamics and functions of the receptors. For example, sialylation and fucosylation of epidermal growth factor receptor (EGFR) has been shown to suppress its dimerization and activation,<sup>1</sup> removal of  $\alpha_{2,6}$ -linked sialic acids from the *N*-linked glycans of the ion channel TRPV5 increases its cell-surface abundance and activity,<sup>2,3</sup> the affinity of  $\alpha_5\beta_1$  integrin was reported to be regulated by sialylation.<sup>4,5</sup> Furthermore, a protein often carries a variety of glycan structures (glycoforms), a phenomenon termed microheterogeneity that frustrates biochemical analysis of purified glycoprotein samples. In addition, glycosylation (e.g., sialylation) can be dynamically regulated on cell surfaces.<sup>6</sup> Therefore, it would be of great interest to visualize *in situ* the glycosylation of a specific receptor of interest on live cells.

However, methods for protein-specific imaging of glycans are largely lacking. Due to the nongenetically encoded nature of glycan biosynthesis, the currently available strategies for imaging glycans such as the metabolic glycan labeling technique enable the visualization of the glycome (i.e., the complete set of glycans),<sup>7</sup> but are incompetent to specifically image the glycoforms of a protein of interest (POI). The metabolic

glycan labeling technique exploits the underlining biosynthetic pathways to metabolically incorporate monosaccharide analogues functionalized with a bioorthogonal functional group (e.g., azide or alkyne). In a second step, the glycans were covalently conjugated with a fluorophore bearing a complementary bioorthogonal functional group. Unlike genetically encoded tools that can tag a specific POI,<sup>8–10</sup> the unnatural monosaccharide is globally incorporated into all glycoproteins and glycolipids containing that sugar. Recently, a transmembrane FRET approach was explored to differentiate the metabolically labeled glycans on a POI by fusing a green fluorescent protein (GFP) to form a FRET pair.<sup>11</sup> However, this strategy suffers from low FRET efficiency because GFP has to be fused to the cytosolic tail of the POI, which is distant from the glycans residing on the other side of the cell membrane.

To overcome these obstacles, we herein report the development of a cis-membrane FRET-based strategy for imaging glycoforms of a specific POI on live cell surfaces (Figure 1). We exploit metabolic glycan labeling in conjunction with site-specific protein labeling to simultaneously install a

Received: October 1, 2013

Published: December 5, 2013

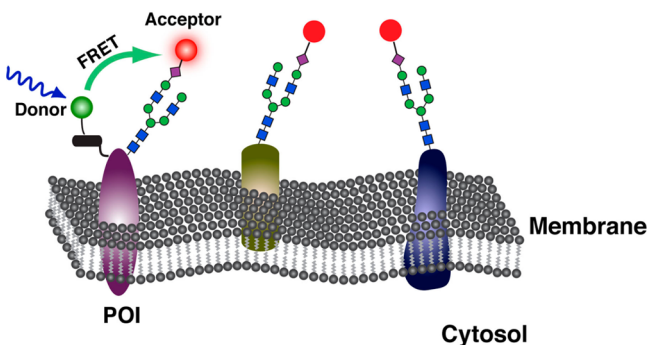


**Figure 1.** Schematic of the FRET-based methodology for protein-specific imaging of cell surface glycans. Various glycans on different cell surface proteins are metabolically labeled with a FRET acceptor, while only the POI is site-specifically tagged with a FRET donor. Since the distance between donor and acceptor must be within ~10 nm, only acceptor bound to the glycans on the same protein is excited through intramolecular FRET, whereas the excess acceptor bound onto other proteins is disfavored.

FRET acceptor and a donor onto the glycans and the extracellular region of the protein scaffold, respectively. The donor and acceptor are both located on the extracellular side (hence termed “cis-membrane”), so that the intramolecular donor–acceptor distance for the POI readily falls within the range for effective FRET (1–10 nm). At the same time, the intermolecular FRET is disfavored since the excess acceptors on other proteins are distant from the donor. As an exemplary combination, we exploited a protein labeling method based on enzyme-catalyzed probe ligation, termed PRIME (probe incorporation mediated by enzymes),<sup>9</sup> to install the FRET donor, and peracetylated *N*-(4-pentynoyl)mannosamine (*Ac*<sub>4</sub>ManNAI)<sup>12</sup> to introduce the FRET acceptor to the sialylated glycans (Figure 2). We demonstrated our strategy by protein-specific imaging of sialylated glycoforms of integrin  $\alpha_X\beta_2$ , which are not amenable to the trans-membrane FRET imaging. Furthermore, our imaging experiments revealed the regulatory functions of glycosylation in  $\alpha_X\beta_2$  activation. Finally, we showed that the cis-membrane FRET method is generally applicable to a variety of cell-surface receptors including EGFR and transforming growth factor-beta receptor type I (T $\beta$ RI).

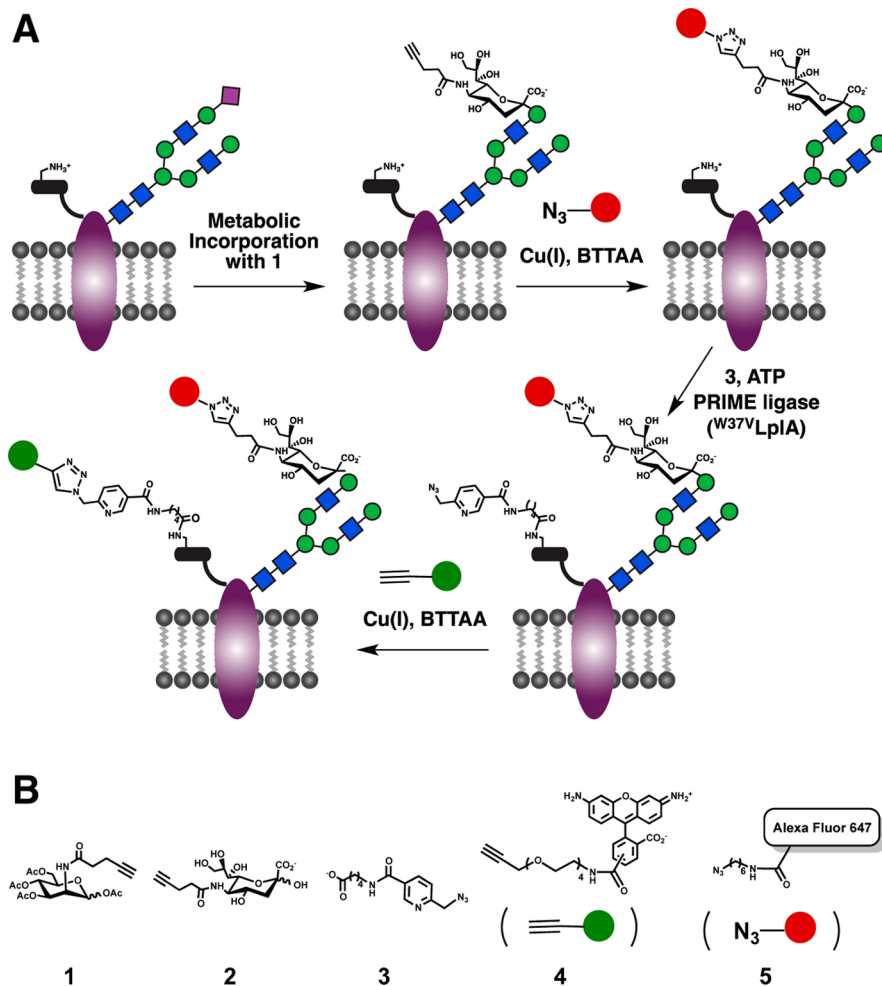


**Figure 2.** Dual-labeling of protein and glycans with two bioorthogonal chemical reporters. (A) Dual-labeling procedure for introducing two bioorthogonal chemical reporters onto protein and glycan, which are conjugated with donor and acceptor, respectively. Cells expressing the POI fused with LAP at the N-termini is incubated with *Ac*<sub>4</sub>ManNAI to introduce SiaNAI into cell-surface sialylated glycans. First, the alkyne-incorporated glycans are reacted with Alexa Fluor 647-azide (FRET acceptor) using CuAAC assisted by BTTAA. Second, LAP was conjugated with the lipoic acid-picoly azide derivative using <sup>W37V</sup>LplA, followed by reaction with Fluor 488-alkyne (FRET donor). (B) Structures of unnatural sugars and probes used in this work: *Ac*<sub>4</sub>ManNAI (1), SiaNAI (2), picolyl azide (3), Alexa Fluor 647-azide (4), and Fluor 488-alkyne (5).

The cis-membrane FRET strategy developed in this work is compatible with other protein labeling methods and may be applied to visualize various types of glycosylation, thus offering a powerful tool for probing how the functions of a POI are regulated by its glycoforms on live cells.

## ■ RESULTS AND DISCUSSION

**Cis-Membrane FRET vs Trans-Membrane FRET.** The FRET efficiency depends on the donor–acceptor separation distance ( $r$ ) with an inverse sixth power and  $r$  has to be within the range of 1–10 nm to warrant effective FRET. For a cell surface receptor, installing the donor–acceptor pair on two different sides of the membrane compromises the FRET efficiency, since the plasma membrane itself possesses a thickness of about 4 nm. Obviously, the cis-membrane FRET configuration is advantageous for ensuring the effectiveness of FRET.

Among the methods for protein labeling and imaging, the genetically encoded GFP and its variant have been most widely used. However, for a cell surface receptor, GFP fusion is largely confined to the cytosolic tail, because fusion to the extracellular tail often impairs protein expression and translocation.<sup>13</sup> GFP is therefore only compatible with the trans-membrane FRET configuration. Nevertheless, trans-membrane FRET between GFP fused to the cytosolic tail and the extracellular glycans labeled with a FRET acceptor might be possible for certain receptors whose glycosylation sites are located relatively close to the cytosolic tail, as previously demonstrated for glycans on EGFR and glucose transporter type 4 (GLUT4).<sup>11</sup> Receptors with large cytosolic domains are intractable to study by trans-membrane FRET. In addition, the relatively large size of GFP tags, even if fused at the cytosolic tail, may cause significant structural perturbation and thus influence the expression, localization, or function of the POI.<sup>14,15</sup>

To achieve the cis-membrane FRET, we employed the PRIME protein labeling method.<sup>9</sup> PRIME utilizes an engineered *Escherichia coli* enzyme lipoic acid ligase (LplA) or its mutants that recognize and ligate lipoic acid derivatives functionalized with an azide onto a transposable 13-amino acid peptide called LAP (LplA Acceptor Peptide). The azide can then be conjugated with an alkyne-containing fluorophore using copper(I)-catalyzed azide–alkyne cycloaddition (CuAAC), a widely used bioorthogonal reaction.<sup>16,17</sup> In our strategy, to the extracellular termini of a cell-surface POI is fused the LAP, which is then conjugated with a lipoic acid derivative containing a picolyl azide moiety using a LplA mutant, <sup>W37 V</sup>LplA (Figure 2). Compared to alkyl azides, the picolyl azide was shown to improve the reaction rate of CuAAC.<sup>18</sup>

**Evaluation of Donor–Acceptor Pairs.** Both the protein labeling and glycan labeling methods employed in our strategy are compatible with small-molecule fluorophores, which are smaller, brighter, and more photostable than GFP. Since the acceptor is present in large excess on the cell surface, i.e., a huge amount of glycans on various proteins are metabolically labeled with acceptor, while only the POI is labeled with donor (Figure 1), the acceptor spectral bleed-through in the FRET channel is the major pitfall to be avoided. To do so, a FRET pair with well-separated excitation spectra is desired so that the direct excitation of the acceptor at the wavelength used to excite the donor, resulting in excess acceptor emission not from FRET, is minimized. By measuring the spectra of several fluorophores, Fluor 488-alkyne and Alexa Fluor 647-azide were found to

fulfill the requirement and were chosen for this work (Figure S1 in Supporting Information [SI]).

**Imaging Integrin  $\alpha_X\beta_2$  Glycans by Cis-Membrane FRET, but Not Trans-Membrane FRET.** Integrins are a major family of  $\alpha\beta$  heterodimeric cell-surface receptors that play important roles in cell adhesion, migration, and proliferation.<sup>19</sup> The  $\beta_2$  integrin subfamily including  $\alpha_D\beta_2$ ,  $\alpha_M\beta_2$ ,  $\alpha_I\beta_2$ , and  $\alpha_Y\beta_2$  are exclusively expressed on leukocytes.  $\beta_2$  integrins mediate leukocyte trafficking in inflammation and binding to antigen-presenting cells.<sup>20</sup> Both  $\alpha$  and  $\beta$  subunits of  $\beta_2$  integrins are type I transmembrane proteins and contain multiple N-linked glycosylation sites. Analysis of the glycans released from  $\beta_2$  integrins revealed oligomannose-, complex-, and hybrid-type N-glycans.<sup>21</sup> Although glycosylation of other integrin subfamilies such as  $\beta_1$  integrins has been well studied,<sup>4,5</sup> the functional roles of  $\beta_2$  integrin glycans remain poorly understood. We therefore sought to visualize the glycoforms of  $\beta_2$  integrins on live cells in a protein-specific manner using the cis-membrane FRET strategy. Notably, the glycans of  $\beta_2$  integrins are not amenable to imaging using the cytosolic GFP fusion method (see detailed comparison and characterization below).

Toward this aim, we fused LAP at the N-termini of the  $\beta_2$  subunit and expressed LAP tagged  $\alpha_X\beta_2$  (LAP- $\alpha_X\beta_2$ ) in HEK 293T cells. The LAP- $\alpha_X\beta_2$ -expressing cells were treated with Ac<sub>4</sub>ManNAI to introduce the alkynyl sialic acid (SiaNAI) into cell-surface sialylated glycans. We then sequentially conjugated the FRET pair onto  $\alpha_X\beta_2$ . First, the alkyne-incorporated glycans, including all that were attached to  $\alpha_X\beta_2$  and other cell-surface proteins, were reacted with the FRET acceptor, Alexa Fluor 647-azide, using CuAAC assisted by the ligand BTTAA.<sup>22</sup> Second, LAP fused to  $\alpha_X\beta_2$  was conjugated with the lipoic acid-picoly azide derivative using <sup>W37 V</sup>LplA, followed by reaction with Fluor 488-alkyne using the BTTAA-assisted CuAAC to serve as the FRET donor (Figure 2). It is noteworthy that there was no detectable cross reaction between the unreacted SiaNAI and the lipoic acid-picoly azide, probably due to the steric hindrance and the presence of picoly azide in large excess (Figure S2 in SI). The strain-promoted azide–alkyne cycloaddition (i.e., the copper-free click chemistry)<sup>23</sup> can also be employed to avoid the possible cross reaction. We next evaluated the cytotoxicity of the labeling procedures by using the MTS cell proliferation assay (Figure S3 in SI). In agreement with the previous studies,<sup>18,22</sup> the BTTAA ligand improved the cellular compatibility of CuAAC to a level comparable to the copper-free click chemistry.

Before performing FRET imaging experiments, we confirmed that  $\alpha_X\beta_2$  was dually labeled with the FRET pair of fluorophores *in vitro* by in-gel fluorescence scanning. The dually labeled cells were lysed, followed by anti- $\beta_2$  immunoprecipitation to isolate  $\alpha_X\beta_2$  protein. Analysis of the immunoprecipitate by in-gel fluorescence scanning indicated that the two fluorophores, donor and acceptor, were simultaneously conjugated to N-termini and sialylated glycans of  $\beta_2$ , respectively (Figure 3A). The  $\beta_2$  protein purified from control cells treated with Ac<sub>4</sub>ManNAI or LAP absent showed only one color. These results proved that the dual-labeling procedure efficiently installed the FRET pairs onto the integrin  $\beta_2$  subunit. On the basis of the ligation efficiency of <sup>W37 V</sup>LplA,<sup>18</sup> the incorporation efficiency of SiaNAI,<sup>24</sup> and the reaction kinetics of the BTTAA-assisted CuAAC,<sup>18,22</sup> we estimated that more than half of the  $\beta_2$  protein was dually labeled with both

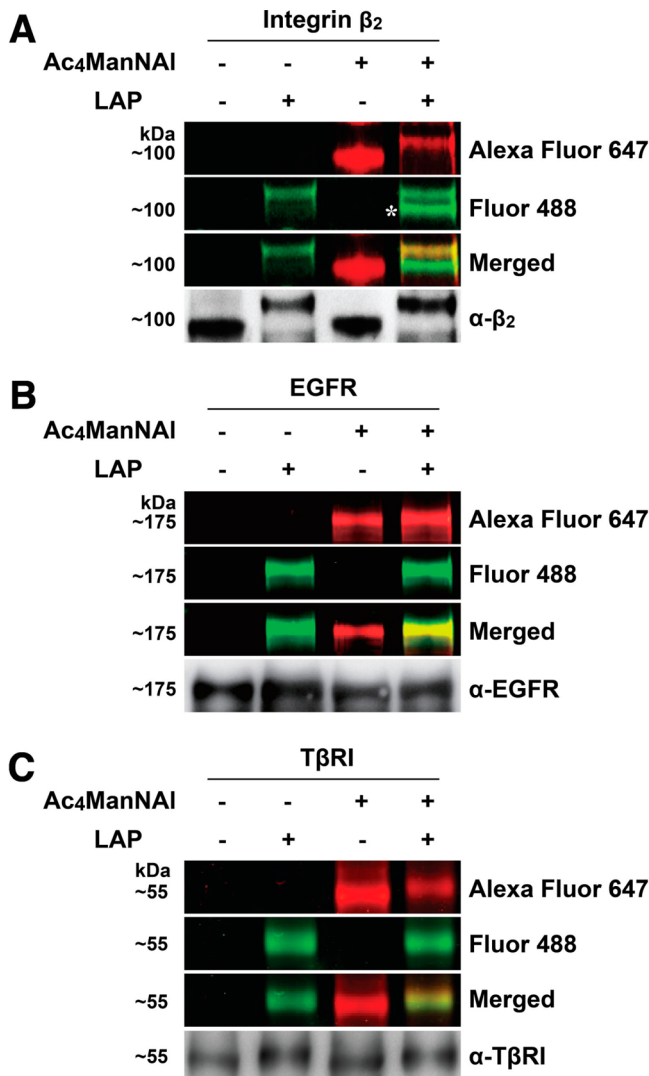


**Figure 3.** In vitro characterization of dually labeled integrin  $\beta_2$  (A), EGFR (B), and T $\beta$ RI (C). HEK 293T cells were transfected with LAP- $\alpha_X\beta_2$ , LAP-EGFR, or LAP-T $\beta$ RI and incubated with 50  $\mu$ M Ac<sub>4</sub>ManNAI for 2 d. The cells were reacted with Alexa Fluor 647-azide to label SiaNAI, followed by two-step PRIME labeling of LAP with Fluor 488-alkyne. Cell lysates were subjected to immunoprecipitation to isolate the labeled integrin  $\beta_2$  (A), EGFR (B), and T $\beta$ RI (C), which were then visualized by fluorescence gel scanning. \* in (A), nonspecific bands.

the donor and acceptor (see the Experimental Section for the estimation procedures).

We next subjected the dually labeled cells to live-cell imaging using confocal FRET microscopy. The images of Fluor 488 fluorescence, Alexa Fluor 647 fluorescence, and FRET-induced fluorescence of the cells are shown (Figure 4 and see Figure S4 in SI for a zoomed-out view of a group of cells). Strong FRET-induced fluorescence signal was observed at the rim of cells transfected with LAP- $\alpha_X\beta_2$  (Figure 4A and Figure S4A in SI), showing the sialylated glycans of  $\alpha_X\beta_2$  on the cell surface. It should be noted that glycans on the  $\alpha_X$  and  $\beta_2$  subunits were both visualized since the two subunits are closely associated. Negative controls with Ac<sub>4</sub>ManNAI (Figure 4C and Figure S4B in SI) or LAP (Figure 4D and Figure S4C in SI) absent showed only Fluor 488 fluorescence or Alexa Fluor 647 fluorescence, respectively, and neither of them showed FRET-induced

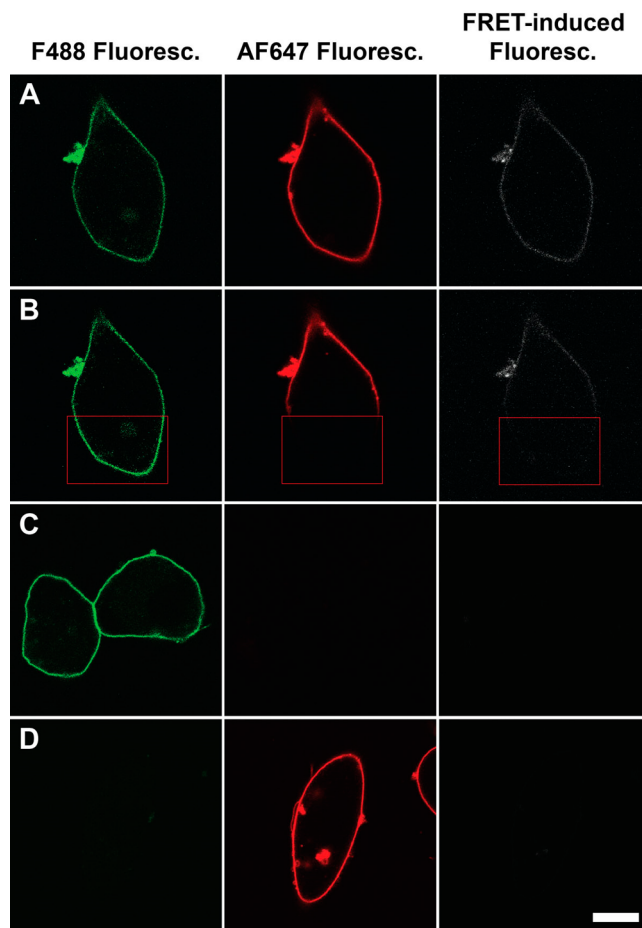


**Figure 4.** Protein-specific imaging of sialylated glycans of integrin  $\alpha_X\beta_2$  on live cells using the cis-membrane FRET-based method. (A) HEK 293T cells expressing LAP- $\alpha_X\beta_2$  were treated with Ac<sub>4</sub>ManNAI, followed by sequential bioorthogonal labeling with donor and acceptor. (B) Donor dequenching after acceptor photobleach. The inserted red box indicates the area photobleached. (C) Negative control in which Ac<sub>4</sub>ManNAI is absent. (D) Negative control in which LAP tag is absent. Left column: Fluor 488 fluorescence (excitation: 488 nm/emission: 505 to 600 nm); middle column: Alexa Fluor 647 fluorescence (excitation: 639 nm/emission: 640 to 700 nm); right column: FRET-induced fluorescence (excitation: 488 nm/emission = 700 nm). Scale bar: 10  $\mu$ m.

fluorescence. Quantitative analysis showed that the intensity of FRET-induced fluorescence of the sialylated glycans of  $\alpha_X\beta_2$  in Figure 4A is more than 40 times higher than the background signal in Figure 4C (Figure S5A in SI).

Furthermore, we collected the fluorescence emission spectrum excited at 488 nm on the cell surfaces (Figure 5). An emission peak at 678 nm was clearly observed on cells with dual-labeled  $\alpha_X\beta_2$  (Figure 5, Spectrum A), corresponding to the FRET-induced fluorescence observed in Figure 4A. Notably, there was essentially no bleed-through signal in the FRET channel resulting from the acceptor spectral, as shown by the absence of fluorescence around 678 nm on the control cells without FRET donor (Figure 5, Spectrum B). These results demonstrate that by choosing a FRET pair with well-separated excitation spectra, the acceptor spectral bleed-through in the FRET channel is satisfactorily avoided, even when the acceptor is in large excess.

**Verification of the Intramolecular FRET-Induced Fluorescence.** To further confirm the FRET-induced

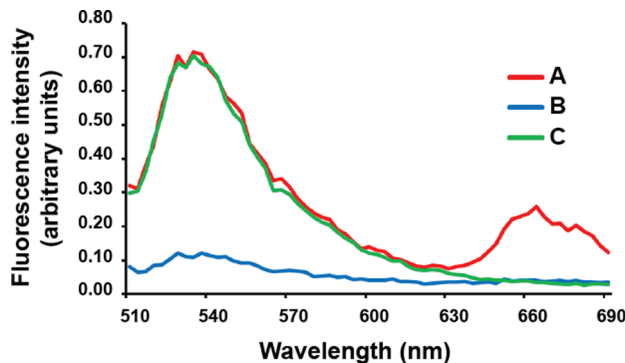


**Figure 5.** Fluorescence emission spectrum excited at 488 nm on the cell surfaces. (A) HEK 293 T cells expressing LAP- $\alpha_X\beta_2$  and dually labeled with donor and acceptor. (B) Cells expressing wild-type  $\alpha_X\beta_2$  with no LAP tag. (C) Cells expressing LAP- $\alpha_X\beta_2$  with no Ac<sub>4</sub>ManNAc.

fluorescence observed in Figure 4A, we performed donor dequenching after acceptor photobleaching, in which the acceptor is bleached using laser irradiation to eliminate FRET quenching and the donor is accessed for the increase of its fluorescence emission. A selected region of the cell was illuminated with a red laser (639 nm) at high-power to completely photobleach Alexa Fluor 647, while keeping the direct bleaching of Fluor 488 donor to a minimum. We observed an increase of donor emission and a complete loss of FRET upon the abolishment of acceptor emission (Figure 4B), indicating that the fluorescence signal of  $\alpha_X\beta_2$  glycans was specifically induced by FRET.

Next, we sought to rule out the possibility of intermolecular FRET by performing two control experiments (Figure 6). First, we expressed a LAP-tagged cell surface protein that is not glycosylated by fusing LAP to the transmembrane (TM) domain of the platelet-derived growth factor receptor. The TM-LAP protein does not possess any glycosylation site and is targeted to the cell surface by TM domain, therefore serving as

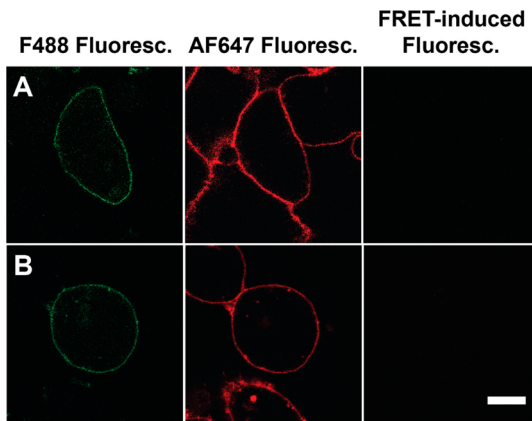


**Figure 6.** Negative control experiments verifying the intramolecular FRET-induced fluorescence of  $\alpha_X\beta_2$  glycoforms. (A) The cells were transfected with LAP-TM that does not possess glycosylation sites. This negative control indicates that intermolecular FRET between LAP and excess acceptor dyes on glycans of nontargeted proteins is negligible. (B) The cells expressing LAP- $\alpha_X\beta_2$  were treated with tunicamycin to inhibit the N-linked glycosylation. No significant intermolecular FRET-induced fluorescence signal was observed between the LAP and the sialic acids on the surrounding O-linked glycans. Scale bar: 10  $\mu$ m.

a nice control where intramolecular FRET is absent. If there were no intermolecular FRET between TM-LAP and the surrounding sialylated glycans on cell surfaces, no FRET would occur. As expected, we observed Fluor 488-labeled TM-LAP and Alexa Fluor 647-labeled glycans individually, but no significant intermolecular FRET between LAP and surrounding glycans was detected (Figure 6A and see Figure S5B in SI for quantitative analysis). Second, we treated the LAP- $\alpha_X\beta_2$ -expressing cells with tunicamycin, an inhibitor that blocks N-linked glycosylation. In this experiment, the N-glycans and hence the sialic acids on integrins were abolished, while there were large amounts of sialic acids remaining on the O-linked glycosylated cell-surface proteins. Similarly, no significant intermolecular FRET between deglycosylated LAP- $\alpha_X\beta_2$  and surrounding O-linked glycans was observed (Figure 6B and see Figure S5B in SI for quantitative analysis).

In the first control experiment, the TM-LAP protein only extends above the plasma membrane with  $\sim$ 30 residues. Some of the sialic acids may locate further away from the cell surface. One way to address the possible false negative results is to vary the length of the linker between TM and LAP. Alternatively, we inhibited the N-linked glycosylation in the second control experiment. It should be noted that sialic acids on the N-glycans of surrounding proteins were also abolished. An ideal control would be to selectively remove the sialic acids on  $\alpha_X\beta_2$ , which is challenging because mutation of the N-linked glycosylation sites usually impair protein folding and translocation to the plasma membrane.<sup>25</sup> Nevertheless, the collective results of the two control experiments strongly support that the FRET-induced fluorescence observed on sialylated glycoforms of integrin  $\alpha_X\beta_2$  is selectively excited through intramolecular FRET and the contribution from the intermolecular FRET is not significant. The cis-membrane FRET-based method can therefore be used for protein-specific glycoform imaging.

**Comparison of the Efficiency between Cis-Membrane FRET and Trans-Membrane FRET.** One of the major advantages of the cis-membrane FRET method is that the donor and acceptor are in close proximity, thus warranting efficient energy transfer. By contrast, the previously reported trans-membrane FRET method<sup>11</sup> may suffer from the distance separation and hence insufficient energy transfer. Integrin  $\beta_2$  contains a flexible cytoplasmic tail with an estimated length of approximately 8 nm.<sup>26</sup> In addition, the thickness of the plasma membrane is about 4 nm. Therefore, we concluded that the glycoforms of  $\beta_2$  integrins were not amenable to the trans-membrane FRET strategy. To verify this conclusion, we fused GFP to the cytosolic terminal of  $\beta_2$ . The  $\alpha_X\beta_2$ -GFP-expressing HEK 293T cells were treated with Ac<sub>4</sub>ManNAc, followed by conjugation with Alexa Fluor 647-azide. Alex Fluor 647 was chosen on the basis of its excitation spectrum well-separated from that of GFP (Figure S6 in SI). The cells were then imaged by trans-membrane FRET (Figure 7 and Figures S7, S8 in SI). Only minimal FRET-induced fluorescence was observed, which was essentially indistinguishable from the background (Figure S7E in SI).

Furthermore, we compared the FRET efficiencies between the trans-membrane and the cis-membrane FRET methods. The FRET efficiencies were measured by donor dequenching after acceptor photobleaching. For integrin  $\alpha_X\beta_2$ , the FRET efficiencies of the trans-membrane and the cis-membrane FRET were  $\sim$ 9% and  $\sim$ 48%, respectively (Figure 7B and Figure S9 in SI). These results demonstrate that the cis-membrane FRET possesses much higher FRET efficiency and

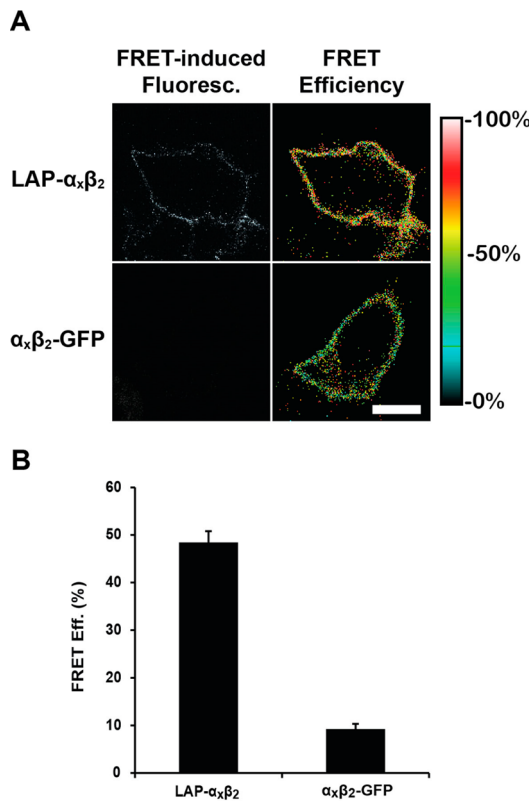


**Figure 7.** Quantitative comparison of the FRET efficiencies between the trans-membrane FRET and the cis-membrane FRET methods. (A) FRET-induced fluorescence imaging and FRET efficiency imaging of HEK 293T cells expressing LAP- $\alpha_X\beta_2$  (top row) and  $\alpha_X\beta_2$ -GFP (bottom row). The FRET efficiency for each pixel was measured by donor dequenching after acceptor photobleaching. A representative individual cell was shown for each row. The color-coded scale is for the FRET efficiencies. The scale bar: 10  $\mu$ m. (B) Averages of the FRET efficiencies measured on 10 individual cells for each experiment. The error bars show SEM.

enables the visualization of glycoforms of POIs such as  $\beta_2$  integrins that are intractable to study by the trans-membrane method.

**Sialylation Is Important for Integrin  $\alpha_X\beta_2$  Activation.** Having established the protein-specific imaging of  $\alpha_X\beta_2$  glycoforms using the cis-membrane FRET method, we therefore investigated the functional roles of sialylation in  $\alpha_X\beta_2$  activation. On cell surfaces,  $\beta_2$  integrins need to be activated in order to bind ligands with high affinity.<sup>19,27,28</sup> The activation involves global conformational rearrangements. Cell-surface integrins adopt an equilibrium between three overall conformational states: the bent conformation, the extended-closed headpiece conformation (the extended integrin with a closed headpiece), and the extended-open headpiece conformation (the extended integrin with an open headpiece).<sup>19</sup> Only the extended-open headpiece conformation has high affinity for ligand binding.<sup>27</sup> Biochemical analysis revealed that  $\beta_2$  integrins contain sialylated N-linked glycans.<sup>21</sup> Interestingly, a RTX cytotoxin, *Bordetella pertussis* CyaA, was shown to recognize the sialylated N-glycans of  $\alpha_M\beta_2$  integrin as the receptor for host infection.<sup>29</sup> Nonetheless, whether the glycosylation affects the  $\beta_2$  integrin activation remains unclear.

To elucidate the functional roles of  $\beta_2$  integrin sialylation, we imaged the changes in sialylation of  $\alpha_X\beta_2$  on live cells and correlated the sialylation states to the integrin activation states

(Figure 8, Figure S10 in SI, and see Figure SSC in SI for quantification). The 293T cells expressing LAP- $\alpha_X\beta_2$  were treated with a fluorinated sialic acid analogue (3F<sub>ax</sub>-Neu5Ac) that inhibits sialylation in cells.<sup>30</sup> FRET imaging revealed that the sialylation of  $\alpha_X\beta_2$  on cell surfaces was almost completely inhibited by 3F<sub>ax</sub>-Neu5Ac. The activation states of  $\alpha_X\beta_2$  were simultaneously visualized by using two  $\beta_2$ -specific monoclonal antibodies (mAbs) that are activation-dependent and can report the activation states of  $\beta_2$  integrins. mAb MEM 148 specifically recognizes the activated extended-open headpiece conformation, while mAb 7E4 reports the inactivated, bent conformation.<sup>27,31,32</sup> Multicolor imaging revealed that MEM 148 recognized the sialylated form of  $\alpha_X\beta_2$ , but could not bind the desialylated  $\alpha_X\beta_2$  (Figure 8A and Figure S10A in SI). By contrast, 7E4 recognized both the sialylated and desialylated  $\alpha_X\beta_2$  (Figure 8B and Figure S10B in SI).

The epitope of MEM 148 maps to residue Pro-374 on the inner face of the  $\beta_2$  hybrid domain,<sup>33</sup> near which there is no N-linked glycosylation site. The imaging results therefore indicate that the removal of sialic acids impairs  $\alpha_X\beta_2$  activation, suggesting a regulatory function of sialylation in  $\beta_2$  integrin activation. However, it should be noted that we cannot completely rule out the possibility that sialic acid is indirectly involved in MEM 148 recognition. More studies to elucidate the detailed mechanism are currently under investigation in our laboratory.

**General Applicability of the Cis-Membrane FRET Method.** To further demonstrate the utility of this method, we extended it to visualize the sialylated glycoforms of another two classes of cell surface receptors, EGFR and T $\beta$ RI. To image the sialylated glycans of EGFR, we expressed EGFR fused with LAP at the N-termini in HEK 293T cells, and treated the cells with Ac<sub>4</sub>ManNAI, followed by dually labeling of cell-surface EGFR. Anti-EGFR immunoprecipitation of the cell lysates, and in-gel fluorescence scanning indicated that the LAP tagged to EGFR was conjugated with Fluor 488 via PRIME, and simultaneously SiaNAI was incorporated into the sialylated glycan of EGFR and reacted with Alexa Fluor 647-azide (Figure 3B). We then performed the cis-membrane FRET imaging of the sialylated glycans of EGFR. Live-cell imaging clearly showed the FRET-induced fluorescence on the plasma membrane resulting from the sialylated glycans of EGFR (Figure 9A, Figure SSD in SI and Figure S11 in SI). The FRET efficiency was quantified to be ~46% (Figure S11 in SI). Similarly, the FRET-induced fluorescent signal was confirmed by performing donor dequenching after acceptor photobleaching experiments (Figure S11B in SI).

Transforming growth factor-beta (TGF- $\beta$ ) signal transduction plays important roles in various cellular processes such as cell growth, migration, and differentiation.<sup>34</sup> Upon binding of TGF- $\beta$  ligand, TGF- $\beta$  receptors type II (T $\beta$ RII) recruits T $\beta$ RI and form a heteromeric complex, which regulates the downstream signal transduction. T $\beta$ RI and T $\beta$ RII possess one and three N-linked glycosylation sites on the extracellular domain, respectively.<sup>35,36</sup> The N-glycosylation<sup>37</sup> and fucosylation<sup>38,39</sup> have been found to be important for their functions, yet the role of sialylation on TGF- $\beta$  receptors remains poorly understood and has not been visualized on live cells. To visualize the sialylated glycans of T $\beta$ RI, HEK 293T cells were transfected with hemagglutinin epitope (HA)-tagged LAP-T $\beta$ RI and simultaneously treated with Ac<sub>4</sub>ManNAI, followed by dually labeling of cell-surface T $\beta$ RI. Anti-HA immunoprecipitation of the cell lysates, and in-gel fluorescence scanning

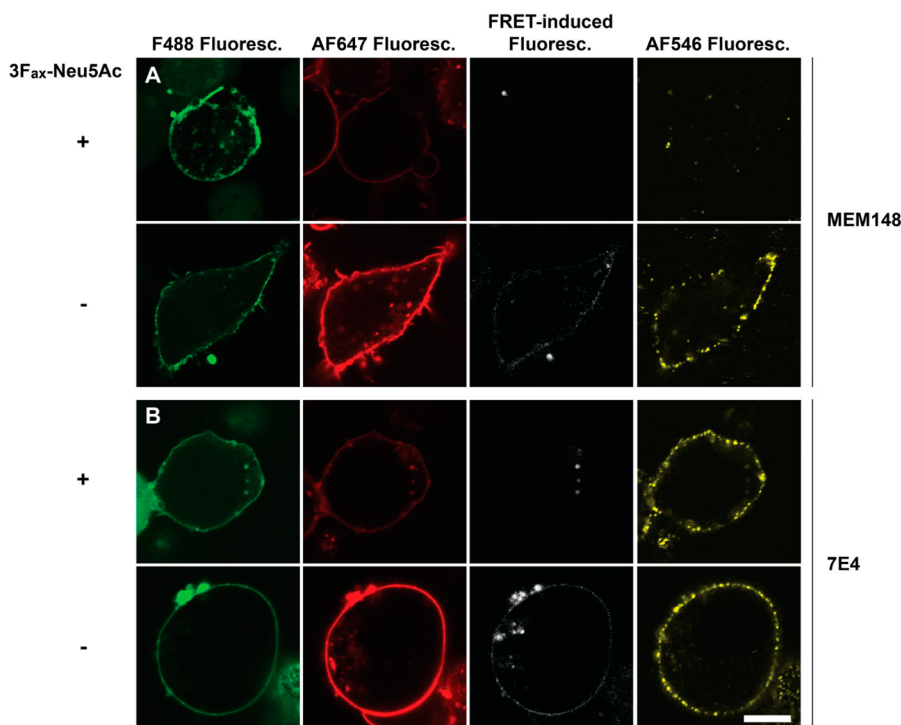


**Figure 8.** Multicolor imaging revealing the functional roles of sialylation in  $\alpha_X\beta_2$  activation. (A) The cells expressing LAP- $\alpha_X\beta_2$  were treated with the sialylation inhibitor 3F<sub>ax</sub>-Neu5Ac (top row) or with vehicle (bottom row). The sialylation of  $\alpha_X\beta_2$  was visualized by the trans-membrane FRET method. The activation states of  $\alpha_X\beta_2$  were visualized by immunofluorescence using MEM 148 and a secondary goat anti-mouse IgG mAb conjugated with Alexa Fluor 546. (B) The activation states of integrin were probed by 7E4 mAb and a secondary goat anti-mouse IgG mAb conjugated with Alexa Fluor 546. Scale bar: 10  $\mu$ m.

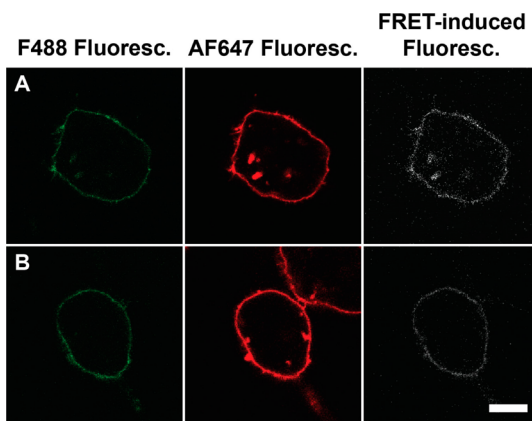


**Figure 9.** Protein-specific imaging of sialylated glycans of EGFR and T $\beta$ RI on live cell. HEK 293T cells expressing LAP-EGFR (A) or LAP-T $\beta$ RI (B) was treated with Ac<sub>4</sub>ManNAI, followed by sequential bioorthogonal labeling with donor and acceptor. The cells were then imaged using the cis-membrane FRET imaging method. Scale bar: 10  $\mu$ m.

showed the dual-labeling of T $\beta$ RI with the donor and acceptor pair (Figure 3C). The cis-membrane FRET imaging exhibited the sialylated glycoform of T $\beta$ RI on cell surface, with a FRET efficiency of  $\sim 50\%$  (Figure 9B, Figure SSE, and Figure S12 in SI).

## CONCLUSION

In conclusion, we present a cis-membrane FRET-based methodology for protein-specific glycan imaging by simultaneously introducing two bioorthogonal chemical reporters onto

the POI and glycans, respectively. The bioorthogonal labeling strategy permits minimal functional perturbation to both proteins and glycans. Our method can potentially be used to image glycoforms of any cell-surface proteins, as exemplified by  $\alpha_X\beta_2$ , EGFR, and T $\beta$ RI in this work. Furthermore, in addition to sialic acid,<sup>40</sup> the metabolic glycan labeling has enabled the visualization of N-acetylgalactosamine (GalNAc)  $\alpha$ -linked to Ser or Thr that is characteristic of mucin-type O-linked glycans,<sup>41</sup> and fucose<sup>42</sup> on live cells. Applying our method to various types of glycosylation will provide new insights into how glycosylation regulates the functions and dynamics of cell surface proteins.

We envision the methodology can be further explored in two aspects. First, protein labeling methods such as the incorporation of the genetically encoded unnatural amino acids (UAs),<sup>10,43</sup> which enable the incorporation of the FRET donor into the sites not limited to the protein termini, can be exploited. PRIME installs the donor on the extracellular region of a POI, but is limited to the terminal. For glycans located far away from the terminal, the UAA method may be advantageous. In addition, UAs in principle can be incorporated into any sites of interest in a site-specific manner, potentially allowing the probing of detailed structural information of the glycosylation sites. Second, the major difficulty for protein-specific imaging of glycoforms is the fact that the acceptor is in large excess. In this work, we overcome this challenge by using the donor–acceptor pair with well-separated excitation spectra. An alternative solution is to use the fluorescence lifetime imaging microscopy (FLIM)-based FRET.<sup>44,45</sup> By measuring the lifetime differences of the donor during FRET, FLIM-FRET is not complicated by the excess donor molecules. Moreover, FLIM-FRET provides better quantification capability. It also

should be noticed that FLIM-FRET, compared to the intensity-based FRET, usually sacrifices some sensitivity and requires more sophisticated instrumentation.<sup>8</sup> We are currently exploring these two directions in our laboratory.

## ■ EXPERIMENTAL SECTION

**Chemical Compounds.** Ac<sub>4</sub>ManNAI (compound 1),<sup>24</sup> picolyl azide (compound 3),<sup>18</sup> and 3F<sub>ax</sub>-NeuSAc<sup>30</sup> were synthesized as previously described. Fluor 488-alkyne (compound 4) was obtained from Click Chemistry Tools (Scottsdale, AZ, United States). Alexa Fluor 647-azide (compound 5) was purchased from Invitrogen (Carlsbad, CA, States).

**Construction of LAP- $\beta_2$ , LAP-EGFR, LAP-T $\beta$ RI, and LAP-TM.** The human  $\beta_2$  and  $\alpha_X$  gene in pCDNA3.1, EGFR gene in pEGFP-N1, and T $\beta$ RI (ALK5) gene in pCMV5 were used. The LAP-tag (GFEIDKVWYDLDA) was introduced at the *Xba*I site between residues S22 and Q23 of  $\beta_2$  signal sequence using the primers 5'- CTA GTC GCG GCT TCG AGA TCG ACA AGG TGT GGT ACG ACC TGG ACG CCG and 5'- CTA GC G GCG TCC AGG TCG TAC CAC ACC TTG TCG ATC TCG AAG CCG CTA. These primers were annealed, phosphorylated with T4 polynucleotide kinase, and ligated into *Xba*I-digested  $\beta_2$  plasmid. For EGFR, the *Nhe*I site was introduced between residues A21 and S22 of signal sequence using the primers 5'- CTA GTC GGG CTG GCT TCG AGA TCG ACA AGG TGT GGT ACG ACC TGG ACG CCG and 5'- CTA GCG GCG TCC AGG TCG TAC CAC ACC TTG TCG ATC TCG AAG CCA GCC CGA. Then we ligated the LAP-tag into *Nhe*I-digested EGFR plasmid, which also removed EGFP from the C terminal of EGFR. For T $\beta$ RI, the *Nhe*I site was introduced between residues A33 and L34 of signal sequence, followed by introducing the LAP-tag into *Nhe*I-digested T $\beta$ RI plasmid. The primers are 5'- CTA GTA GCG GCT TCG AGA TCG ACA AGG TGT GGT ACG ACC TGG ACG CCG and 5'- CTA GCG GCG TCC AGG TCG TAC CAC ACC TTG TCG ATC TCG AAG CCG CCA. For LAP-TM, the LAP-tag insert containing *Bgl*II and *Sac*II sites was produced by annealing the primers 5'- GAT CTG GCG GCG GCT TCG AGA TCG ACA AGG TGT GGT ACG ACC TGG ACG CCG CTA GCC CGC and 5'- GGG CTA GCG GCG TCC AGG TCG TAC CAC ACC TTG TCG ATC TCG AAG CCG CCG CCA. The insert was then ligated into *Bgl*II- and *Sac*II-digested pDisplay vector (Invitrogen).

**Cell-Surface Glycoprotein Dual-Labeling.** The HEK 293T cells were cultured in DMEM medium containing 100  $\mu$ M Ac<sub>4</sub>ManNAI for 24 h to ~60% confluence and transfected with expression plasmids for LAP- $\alpha_X\beta_2$ , LAP-EGFR, LAP-T $\beta$ RI, or LAP-TM using X-tremeGENE (Roche). After 5 h of transfection, the medium was changed to fresh medium containing Ac<sub>4</sub>ManNAI, followed by culturing in 37 °C for 48 h. The cells were then washed three times with PBS containing 1% FBS, followed by adding of PBS containing 50  $\mu$ M Alexa Fluor 647-azide, 2.5 mM sodium ascorbate, and BTTAA-CuSO<sub>4</sub> complex (50  $\mu$ M CuSO<sub>4</sub>, BTTAA:CuSO<sub>4</sub> in a 6:1 molar ratio) at rt. After 10 min, the cells were washed three times with PBS containing 1% FBS, followed by incubation with purified <sup>W37</sup>VlpIA (10  $\mu$ M, prepared as previously described<sup>9</sup>), picolyl azide (3) (200  $\mu$ M), ATP (1 mM), and Mg(OAc)<sub>2</sub> (5 mM) in cell growth medium for 20 min at rt. After washing three times with PBS containing 1% FBS, the cells were treated with PBS containing 50  $\mu$ M Fluor 488-alkyne, 2.5 mM sodium ascorbate, and BTTAA-CuSO<sub>4</sub> complex (50  $\mu$ M CuSO<sub>4</sub>, BTTAA:CuSO<sub>4</sub> in a 6:1 molar ratio) at rt for 10 min, followed by three washes before being used for the following experiments. For imaging experiments, the cells were cultured in 8-well Chamber slides. For immunoprecipitation, the cells were cultured in 10-cm dishes. For control experiments, the cells were transfected with the corresponding plasmid constructs or cultured in the absence of Ac<sub>4</sub>ManNAI and similarly labeled.

The percentage of the total protein that is simultaneously labeled with both the donor and acceptor is estimated on the basis of the following data: (i) the efficiency of the enzymatic ligation of picolyl azide onto LAP was reported to be 81%;<sup>18</sup> (ii) the metabolic incorporation percentage of SiaNAI in HEK 293T cells was reported

to be 46%.<sup>24</sup>  $\alpha_X\beta_2$  and EGFR contain multiple glycosylation sites. Although T $\beta$ RI contains only one N-linked glycosylation site, it probably contains more than one sialic acid residue on the glycan terminal. It is therefore reasonable to assume every protein contains at least one SiaNAI; (iii) According to the kinetic studies of the BTTAA-assisted CuAAC,<sup>18,22</sup> the reaction proceeds to completion within 5 min. Taken together, we estimated that more than 50% of the LAP-tagged proteins were dually labeled with the FRET donor–acceptor pair in our experimental conditions.

**Immunostaining of  $\alpha_X\beta_2$  on Live Cells.** For sialylation inhibition, cells were treated with 3F<sub>ax</sub>-NeuSAc at 200  $\mu$ M for 72 h. The cells were then subjected to transfection and dual-labeling with the FRET donor and acceptor as described. After washing, the cells were incubated with MEM 148 or 7E4 in PBS buffer containing 10% FBS at 37 °C for 30 min. After washing three times with PBS, the cells were incubated with Alexa Fluor 546-conjugated goat anti-mouse antibody (5  $\mu$ g/mL) at rt for 30 min, followed by washing three times with PBS before imaging.

**Immunoprecipitation.** The labeled cells were lysed with 0.5 mL of ice-cold lysis buffer (20 mM Tris, pH 8.0, 400 mM NaCl, 10% glycerol, 0.2% Triton X-100, 1 mM EDTA, 0.1 mM DTT, 1× complete protease inhibitor cocktail). Cell lysates were collected after centrifuging at 10000g for 5 min at 4 °C to remove cell debris.  $\beta_2$  and LAP- $\beta_2$ , were immunoprecipitated using anti- $\beta_2$  antibody (7E4, 1  $\mu$ g/sample) and pulled down by Protein A/G-agarose beads (Santa Cruz SC-2003). EGFR and LAP-EGFR proteins were immunoprecipitated using anti-EGFR antibody (1  $\mu$ g/sample, Oncogene GR01L) and pulled down by Protein A/G-agarose beads. HA-tagged T $\beta$ RI and LAP-T $\beta$ RI proteins were immunoprecipitated by incubating with anti-HA mAb-magnetic beads (MBL M180-9) overnight at 4 °C. The agarose beads or magnetic beads were washed three times with PBS, followed by heating in SDS-loading buffer for 5 min at 95 °C to release the proteins.

**In-Gel Fluorescence Scanning and Immunoblotting.** Proteins separated by SDS-PAGE were visualized by first incubating the gel in destaining solution (50% methanol, 40% H<sub>2</sub>O, 10% acetic acid) with shaking for 5 min, followed by washing in water for 5 min and directly scanning the gel on an Amersham Biosciences Typhoon Trio+ variable mode imager (excitation 488 nm/520 nm filter, 40 nm band-pass for Fluor 488 and excitation 633 nm/670 nm filter, 30 nm band-pass for Alexa Fluor 647). For Western blotting, proteins were blotted by primary antibodies (anti- $\beta_2$  mouse monoclonal antibody, MEM 148, 1:2000; anti-EGFR rabbit monoclonal antibody (Epitomics 1902-1), 1:2000; anti-T $\beta$ RI rabbit polyclonal antibody (Santa Cruz sc-9048), 1:1000) followed by goat anti-mouse-HRP or goat anti-rabbit-HRP conjugated secondary antibody.

**Fluorescence Imaging.** Live cell fluorescence and FRET imaging was performed on a Zeiss LSM 700 laser scanning confocal microscope equipped with a 63X oil immersion objective lens (N.A. 1.4). Fluor 488 fluorescence was excited using a 488-nm line of solid-state laser and collected with a 505- to 600-nm band-pass filter. Alexa Fluor 647 fluorescence was excited using a 639-nm line of solid-state laser and collected with a 640-nm long-pass filter. FRET-induced fluorescence was excited using the 488-nm laser and collected with the 640-nm long-pass filter. Fluor 546 fluorescence was excited using a 555-nm line of solid-state laser and collected with a 570- to 610-nm band-pass filter. The fluorescence emission spectra of cells were taken on a Leica SP8X laser scanning confocal microscope, using a pulsed white light laser (WLL) (excited at 488 nm). The emission was collected from 510- to 690-nm using a 3-nm step.

## ■ ASSOCIATED CONTENT

### S Supporting Information

Supplementary figures. This material is available free of charge via the Internet at <http://pubs.acs.org>.

## ■ AUTHOR INFORMATION

### Corresponding Author

xingchen@pku.edu.cn

**Notes**

The authors declare no competing financial interest.

**ACKNOWLEDGMENTS**

We thank A. Ting for the LplA plasmid, Y. Chen for the EGFR and T $\beta$ RI plasmids, and Dr. L. Feng and Mr. B. Cheng for help on chemical synthesis. This work was supported by the National Basic Research Program of China (973 Program) (No. 2012CB917303) and the National Natural Science Foundation of China (No. 91313301, and No. 91127034).

**REFERENCES**

- (1) Liu, Y.-C.; Yen, H.-Y.; Chen, C.-Y.; Chen, C.-H.; Cheng, P.-F.; Juan, Y.-H.; Chen, C.-H.; Khoo, K.-H.; Yu, C.-J.; Yang, P.-C.; Hsu, T.-L.; Wong, C.-H. *Proc. Natl. Acad. Sci. U.S.A.* **2011**, *108*, 11332.
- (2) Chang, Q.; Hoefs, S.; van der Kemp, A. W.; Topala, C. N.; Bindels, R. J.; Hoenderop, J. G. *Science* **2005**, *310*, 490.
- (3) Cha, S.-K.; Ortega, B.; Kurosu, H.; Rosenblatt, K. P.; Kuro-O, M.; Huang, C.-L. *Proc. Natl. Acad. Sci. U.S.A.* **2008**, *105*, 9805.
- (4) Zhuo, Y.; Chammas, R.; Bellis, S. L. *J. Biol. Chem.* **2008**, *283*, 22177.
- (5) Semel, A. C.; Seales, E. C.; Singhal, A.; Eklund, E. A.; Colley, K. J.; Bellis, S. L. *J. Biol. Chem.* **2002**, *277*, 32830.
- (6) Cohen, M.; Varki, A. *OMICS: J. Integrative Biol.* **2010**, *14*, 455.
- (7) Laughlin, S. T.; Bertozzi, C. R. *Proc. Natl. Acad. Sci. U.S.A.* **2009**, *106*, 12.
- (8) Zhang, J.; Campbell, R. E.; Ting, A. Y.; Tsien, R. Y. *Nat. Rev. Mol. Cell Biol.* **2002**, *3*, 906.
- (9) Fernández-Suárez, M.; Baruah, H.; Martínez-Hernández, L.; Xie, K. T.; Baskin, J. M.; Bertozzi, C. R.; Ting, A. Y. *Nat. Biotechnol.* **2007**, *25*, 1483.
- (10) Hao, Z.; Hong, S.; Chen, X.; Chen, P. R. *Acc. Chem. Res.* **2011**, *44*, 742.
- (11) Haga, Y.; Ishii, K.; Hibino, K.; Sako, Y.; Ito, Y.; Taniguchi, N.; Suzuki, T. *Nat. Commun.* **2012**, *3*, 907.
- (12) Hsu, T.-L.; Hanson, S. R.; Kishikawa, K.; Wang, S.-K.; Sawa, M.; Wong, C.-H. *Proc. Natl. Acad. Sci. U.S.A.* **2007**, *104*, 2614.
- (13) Brock, R.; Hamelers, I. H.; Jovin, T. M. *Cytometry* **1999**, *35*, 353.
- (14) Hoffmann, C.; Gaietta, G.; Bünenmann, M.; Adams, S. R.; Oberdorff-Maass, S.; Behr, B.; Vilardaga, J.-P.; Tsien, R. Y.; Ellisman, M. H.; Lohse, M. J. *Nat. Methods* **2005**, *2*, 171.
- (15) Yao, X.; Parnot, C.; Deupi, X.; Ratnala, V. R. P.; Swaminath, G.; Farrens, D.; Kobilka, B. *Nat. Chem. Biol.* **2006**, *2*, 417.
- (16) Rostovtsev, V. V.; Green, L. G.; Fokin, V. V.; Sharpless, K. B. *Angew. Chem., Int. Ed.* **2002**, *41*, 2596.
- (17) Bertozzi, C. R. *Acc. Chem. Res.* **2011**, *44*, 651.
- (18) Uttamapinant, C.; Tangpeerachaikul, A.; Grecian, S.; Clarke, S.; Singh, U.; Slade, P.; Gee, K. R.; Ting, A. Y. *Angew. Chem., Int. Ed.* **2012**, *51*, 5852.
- (19) Luo, B.-H.; Carman, C. V.; Springer, T. A. *Annu. Rev. Immunol.* **2007**, *25*, 619.
- (20) Springer, T. A. *Cell* **1994**, *76*, 301.
- (21) Asada, M.; Furukawa, K.; Kantor, C.; Gahmberg, C. G.; Kobata, A. *Biochemistry* **1991**, *30*, 1561.
- (22) Besanceney-Webler, C.; Jiang, H.; Zheng, T.; Feng, L.; Soriano Del Amo, D.; Wang, W.; Klivansky, L. M.; Marlow, F. L.; Liu, Y.; Wu, P. *Angew. Chem., Int. Ed.* **2011**, *50*, 8051.
- (23) Agard, N. J.; Prescher, J. A.; Bertozzi, C. R. *J. Am. Chem. Soc.* **2004**, *126*, 15046.
- (24) Chang, P. V.; Chen, X.; Smyrniotis, C.; Xenakis, A.; Hu, T.; Bertozzi, C. R.; Wu, P. *Angew. Chem., Int. Ed.* **2009**, *48*, 4030.
- (25) Helenius, A. *Science* **2001**, *291*, 2364.
- (26) Campbell, I. D.; Humphries, M. J. *Cold Spring Harbor Perspect. Biol.* **2011**, *3*:a004994.
- (27) Chen, X.; Xie, C.; Nishida, N.; Li, Z.; Walz, T.; Springer, T. A. *Proc. Natl. Acad. Sci. U.S.A.* **2010**, *107*, 14727.
- (28) Nishida, N.; Xie, C.; Shimaoka, M.; Cheng, Y.; Walz, T.; Springer, T. A. *Immunity* **2006**, *25*, 583.
- (29) Morova, J.; Osicka, R.; Masin, J.; Sebo, P. *Proc. Natl. Acad. Sci. U.S.A.* **2008**, *105*, 5355.
- (30) Rillahan, C. D.; Antonopoulos, A.; Lefort, C. T.; Sonon, R.; Azadi, P.; Ley, K.; Dell, A.; Haslam, S. M.; Paulson, J. C. *Nat. Chem. Biol.* **2012**, *8*, 661.
- (31) Drbal, K.; Angelisová, P.; Černý, J.; Hilgert, I.; Horejsí, V. *Immunobiology* **2001**, *203*, 687.
- (32) Tan, S. M.; Robinson, M. K.; Drbal, K.; van Kooyk, Y.; Shaw, J. M.; Law, S. K. *J. Biol. Chem.* **2001**, *276*, 36370.
- (33) Tang, R.-H.; Tng, E.; Law, S. K. A.; Tan, S.-M. *J. Biol. Chem.* **2005**, *280*, 29208.
- (34) Wu, M. Y.; Hill, C. S. *Dev. Cell* **2009**, *16*, 329.
- (35) Ebner, R.; Chen, R. H.; Shum, L.; Lawler, S.; Zioncheck, T. F.; Lee, A.; Lopez, A. R.; Deryck, R. *Science* **1993**, *260*, 1344.
- (36) Tomoda, T.; Kudoh, T.; Noma, T.; Nakazawa, A.; Muramatsu, M.; Arai, K. *Biochem. Biophys. Res. Commun.* **1994**, *198*, 1054.
- (37) Kim, Y.-W.; Park, J.; Lee, H.-J.; Lee, S.-Y.; Kim, S.-J. *Biochem. J.* **2012**, *445*, 403.
- (38) Wang, X.; Inoue, S.; Gu, J.; Miyoshi, E.; Noda, K.; Li, W.; Mizuno-Horikawa, Y.; Nakano, M.; Asahi, M.; Takahashi, M.; Uozumi, N.; Ihara, S.; Lee, S. H.; Ikeda, Y.; Yamaguchi, Y.; Aze, Y.; Tomiyama, Y.; Fujii, J.; Suzuki, K.; Kondo, A.; Shapiro, S. D.; Lopez-Otin, C.; Kuwaki, T.; Okabe, M.; Honke, K.; Taniguchi, N. *Proc. Natl. Acad. Sci. U.S.A.* **2005**, *102*, 15791.
- (39) Lin, H.; Wang, D.; Wu, T.; Dong, C.; Shen, N.; Sun, Y.; Sun, Y.; Xie, H.; Wang, N.; Shan, L. *Am. J. Physiol. Renal Physiol.* **2011**, *300*, F1017.
- (40) Saxon, E.; Bertozzi, C. R. *Science* **2000**, *287*, 2007.
- (41) Hang, H. C.; Yu, C.; Kato, D. L.; Bertozzi, C. R. *Proc. Natl. Acad. Sci. U.S.A.* **2003**, *100*, 14846.
- (42) Sawa, M.; Hsu, T.-L.; Itoh, T.; Sugiyama, M.; Hanson, S. R.; Vogt, P. K.; Wong, C.-H. *Proc. Natl. Acad. Sci. U.S.A.* **2006**, *103*, 12371.
- (43) Liu, C. C.; Schultz, P. G. *Annu. Rev. Biochem.* **2010**, *79*, 413.
- (44) Wallrabe, H.; Periasamy, A. *Curr. Opin. Biotechnol.* **2005**, *16*, 19.
- (45) Becker, W. J. *Microsc.* **2012**, *247*, 119.